Conformational Dynamics of Hyaluronan in Solution. 1. A ^{13}C NMR Study of Oligomers[⊥]

F. Cavalieri,[†] E. Chiessi,[†] M. Paci,[†,§] G. Paradossi,*[,†,‡] A. Flaibani,[#] and A. Cesàro*[,∥]

Department of Chemistry Science and Technology, University of Rome "Tor Vergata", 00133 Rome, Italy; Section B of I.N.F.M. Roma-II, 00133 Rome, Italy; Section B of I.N.F.M. Roma-I, 00185 Rome, Italy; POLY-tech, Area Science Park, Padriciano 99, 34012 Trieste, Italy; and Department of Biochemistry, Biophysics, and Macromolecular Chemistry, University of Trieste, 34127 Trieste, Italy

Received June 20, 2000; Revised Manuscript Received August 16, 2000

ABSTRACT: Conformational dynamic properties of a series of hyaluronan oligomers $(UA)_n$, with degree of polymerization $n = 2-6$, have been investigated through extensive NMR experiments. Dynamic parameters T_1, NOEF (by gated decoupling experiments), and T_2 (by line broadening experiments) on these samples have been collected and analyzed in terms of several averaging procedures aimed at discriminating the ring position in the chain and the carbon type in the ring units U and A. Trends of these parameters and changes of carbon resonance pattern as a function of the oligomer degree of polymerization *n* have been interpreted in terms of changes in the local dynamics of the probe in the conformational fluctuations mainly due to the soft torsional angles at the glycosidic linkages. Preliminary molecular dynamics results on two oligomers $(UA)_2$ and $(UA)_4$ are used to disclose the complex variations which affect the dynamic features of the oligomers, upon increasing degree of polymerization.

Introduction

Ever since the discovery of hyaluronan (HA), its relevance in nature has been emphasized and has recently been reported in many reviews.[1,2] There are several aspects of the structure and properties of HA which make this molecule an interesting subject for investigation. It has a relatively simple regular structure, being an alternating copolymer with a disaccharide (U,A) repeat unit, {→4)-*β*-D-glucuronate-(1→3)-2-deoxy-2-acetamido-*β*-D-glucose-(1→}, and it plays a very important role in biological tissue.

Many physicochemical properties of high molecular weight hyaluronan in dilute solution have been consistently interpreted on the basis of random- or wormlike coils with moderate stiffness.[3,4] Stiffness parameters, such as the persistence length and Kuhn length of about 4−5 nm and 22 nm, respectively, have been estimated from experimental data of scattering and intrinsic viscosity.[5] These conclusions have been recently confirmed on a series of HA fractions ranging in molecular weight from 10^3 to 10^5, suggesting that the wormlike chain model with an "unmistakable semiflexibility" can be applied to this polymer.[6] Other authors[7] have examined the conformational and rheological properties of hyaluronan solutions at different values of concentration, pH, ionic strength, and molecular weight, to shed light on the effects that might arise from conformational ordering by the other more general polymer solution properties. The early results, based on CD, ORD, and viscosity measurements,[8] show that local conformation variations rather than any apparent cooperative[9] changes can be induced in the chain with different counterions. This and other studies suggested that the factors which dictate conformation and packing in solid state influence the hyaluronan chain in solution (i.e., nature of the counterion, pH, degree of hydration). Support comes from the three groups of allomorphs observed in the solid state under the different influences of cations, humidity or both. All the conformational structures are left-handed helices and include 4-fold and 3-fold helices with an axial parameter ranging from 0.85 to 0.95 nm per disaccharide (for an overview see ref 10).

Despite the apparently normal polymer behavior, "stickiness" of HA chains has been observed in solution (network-forming and laterally aggregating behavior) and this has been ascribed to in-registry intermolecular and intramolecular interactions between the polysaccharide chains (cellulose-like). It has therefore been proposed that the secondary structure of hyaluronan in aqueous solution is stabilized by an extensive hydrogen-bonding network which gives the polymer an overall expanded coil structure in solution, as proposed by Scott.[11] It has also been suggested that interresidue hydrogen bonds contribute to intramolecular conformational ordering and also promote a clustering of hydrophobic groups which forms the basis for chain−chain intermolecular interactions in the tertiary structure. A dependence of the weak intermolecular associations of short segments on hyaluronan concentration and a capability for intermolecular association by larger hyaluronan segments have also been indicated.[12]

The weakly charged polyelectrolytic character is another complex feature of HA, inasmuch as the linear charge density is only 0.72 for the fully charged chain, well below the critical counterion condensation threshold[13] for monovalent cations, but not for divalent cations. Reed and co-workers[14,15] interpreted their static and dynamic light scattering data for hyaluronan dilute solutions at different pH values in terms of the poly-

[⊥] Presented in part at the International Symposium "*Redefining Hyaluronan*", Praglia, Italy, June 1999.

* Authors for correspondence. E-mail: G.P., paradossi@stc.uniroma2.it; A.C., cesaro@univ.trieste.it.

[†] University of Rome "Tor Vergata".

[§] Section B of I.N.F.M. of Roma-II.

[‡] Section B of I.N.F.M. of Roma-I.

[#] POLY-tech, Area Science Park.

[∥] University of Trieste.

10.1021/ma001076i CCC: $20.00
Published on Web 12/08/2000

electrolyte properties and their tendency to form aggregates. In solution free of added electrolyte, HA forms stable, polydisperse, entangled aggregates which remain stable for weeks at a time, while in solutions of medium to high ionic strength, most of these aggregates disentangle within days. The same authors subsequently found that the scattered intensity of hyaluronan solutions increased markedly with ionic strength, while the radius of gyration decreased. The total apparent persistence length varied from about 8.7 nm in the high ionic strength limit to nearly 40 nm at 1 mM added NaCl,[15] and this was considered to be consistent with the earlier knowledge of local stiffening due to hydrogen bonding. However, the physical reasons for its conformational versatility still elude a full molecular understanding.

Very recently, MD simulation studies have been carried out[16] in which the conformational freedom of hyaluronan di- and tetrasaccharides has been compared with available NMR data. In one paper, the importance of the hydrogen-bonding network was stressed, based both on direct intramolecular hydrogen bonding and through water caging around the glycosidic linkage. Another paper[17] suggested a detailed topological structure for the high molecular weight HA and unfractionated low molecular weight HA fragments in aqueous solution obtained by combining local structural information gained by the study of ^{13}C NMR with X-ray fiber diffraction data. A detailed NMR study[18] of the effects of various environmental conditions on the conformation of oligomeric and polymeric HA was able to discriminate between the (greater) sensitivity of the β-1,3 and the lesser sensitivity of the β-1,4 linkage. The authors concluded that the conformational versatility[10] of HA is therefore related mainly to the averaging of conformational states at the β-1,3 linkage.

The above summary is considered necessary in order to stress the importance of these studies which have provided the intrinsic key to revealing the molecular properties of this unique versatility of HA. From this overview of the concepts on which the present knowledge of the HA conformation is based, the impression is that, until now, the gap between the local intraresidue conformational dynamics and the overall chain conformational shape has not been filled. On the basis of simplistic statistical considerations, the persistence of connective intraresidue bridges, as proposed on the basis of these recent studies, up to commensurate oligomers does not appear to be straightforward, unless highly cooperative interactions are claimed. The main difficulty is the availability of both experimental dynamic data on suitable oligomers (longer than a tetrasaccharide) and dynamic simulation data on the whole series of homologues, from the short tetrasaccharide to the high M_w chains.

This paper presents detailed experimental results on dynamic parameters determined by ^{13}C NMR on a series of oligomers from the tetrasaccharide $(U-A)_2$ to the dodecasaccharide $(U-A)_6$, together with some preliminary MD investigation. In a forthcoming work, more extensive MD calculations will be compared with the theoretical analysis of the local dynamic behavior, based on a novel application of the optimized Rouse−Zimm local dynamics (ORZLD) to the realistic polysaccharide chain conformation.[19] This approach seems suitable to expand the results of the MD simulations (otherwise cost-prohibitive) to large chain dimensions. The work is part of a project aiming at correlating experimentally determined relaxation properties and configurationally averaged chain dynamics for several oligo- and polysaccharides structures.[19]

Materials and Methods

Preparation of HA Oligosaccharides. Purified rooster comb hyaluronic acid (600 mg, FIDIA, Abano Terme, Italy) was dissolved in 25 mL of aqueous 0.15 M NaCl, buffered with NaOAc/HOAc 10 mM, pH 5.0. The solution was allowed to equilibrate at 37 °C for 30 min before the addition of 64 units of bovine testicular hyaluronidase (SIGMA, type IV−S) per mL of HA. After 20 h of digestion at 37 °C, a further addition of 88 units of enzyme per mL of solution was made. After 40 h, the digestion was stopped by inactivating the enzyme at 100 °C for 10 min. The precipitate was removed by centrifugation for 20 min. The resulting oligosaccharide mixture was applied to a Bio-Gel P6 column (2.6 × 150 cm) which had been preequilibrated with 0.1 M NaCl, 5 mM acetate buffer, pH 5, at flow rate of 30 mL/h. The eluate was monitored with a refractive index detector (Waters differential refractometer R403). Fractions corresponding to tetra-, hexa-, octa-, and decasaccharide were pooled and desalted on a Sephadex G-10 (l.5 × 40 cm). Oligosaccharides higher than decasaccharide were not resolved and the corresponding fractions were pooled together, $(UA)_n$ with $n \geq 6$). The oligosaccharide structure was confirmed by ^{1}H NMR. Fractions were stored as freeze-dried powder.

NMR Measurements. Oligosaccharide samples were dissolved in deuterated water at 5% (w/w), filtered and placed in a 10 mm NMR tube. A Bruker AM400 spectrometer was used at a ^{13}C frequency of 100.6 MHz. NMR spectra were collected at 30 ± 0.1 °C, after a 90° pulse over a size of 128K, FT transformed with a line broadening of 1.2 Hz, and referenced with respect to TMS. T_1 and NOEF were measured by the gated decoupling technique pulse sequence[20] for simultaneous determination of T_1 and NOEF in ^{13}C NMR. T_1 measurements were carried out ensuring a repetition time of longer than $5T_1$. The sequence consists of a repetition rate of about 10.0 s to which acquisition time and presequence delay (about 6.0 s) must be added. After eight dummy scans, 128 transients were acquired. The S/N ratio was optimized with respect to the requirements of long relaxation delays and of possible sample depolymerization. The intensity of magnetization upon delay time was evaluated by direct integration for single peaks and by half integration of the free edge of the resonances or by measuring directly the peak heights in the cases of partially or strongly overlapping peaks, respectively. NOEF values have been obtained by difference between the irradiated acquisition and that obtained after a complete relaxation of the protons. Transverse relaxation time values, T_2, have been obtained by line width at half-height measurement in enlarged spectrum, transformed with a zero filled to 256K and without line broadening. Although reported in the columns of Figure 2, they were not used in the analysis of dynamic data as their evaluation is affected by large uncertainties. Errors on T_1 and NOEF parameters were evaluated to within 10% and 20%, respectively, and refer to the standard deviations for the values of individual carbon atoms. Averages of the experimental values of NOEF and T_1 were made over the five carbon atoms of the sugar ring, ruling out the C6 and the methyl group of the acetamido residue.

Simulation Procedures. Molecular dynamic simulations in vacuo were performed with CHARMm,[21] version c26β1. Parameters and partial charges were taken by adopting a force-field proposed for carbohydrates,[22] with a proteinlike parametrization for carboxyl and *N*-acetylamino groups. Oligosaccharides were modeled with uncharged uronic residues, by simulating a complete screening by counterions. Hydrogen bonding was modeled by adjusting the atomic partial charges and van der Waals parameters for the hydrogen-bond donor and acceptor atoms.[23] A unity value for dielectric constant was used throughout the calculations and long-range interactions

were adjusted to approach zero smoothly by using a switching function applied on a group-by-group basis between 1.0 and 1.2 nm.[23] The starting conformation for the two oligomers was taken from the HA sodium salt structure proposed from fiber diffraction,[24] after a conjugate gradient minimization. Molecular dynamic trajectories were integrated using a Verlet integrator[25] with a time-step of 1 fs. Bond lengths involving hydrogen atoms were kept fixed by using the SHAKE constraint algorithm.[26] Trajectories started with initial velocity components for each atom selected randomly from a thermal distribution. The system was heated through a series of successive reassignments of the atomic velocities followed by dynamic sequences, starting at 60 K and incrementing by 60 K at 2 ps intervals until a temperature of 300 K was reached. The trajectories were then equilibrated at 300 K with periodic scaling if the system temperature deviated from the chosen 300 K by more than 3 K, averaged over the previous 2 ps. After a period of 20 ps of heating and equilibration dynamics, a further 100 ps of free dynamics were required to reach thermal equilibration, as judged by the time series of RMSD for the conformations.[27] The trajectories were afterward integrated for a total of 700 ps. The glycosidic torsion angles φ and ψ were defined as H1−C1−O1−CX and C1−O1−CX−HX, respectively, where X is 3 or 4, depending on linkage type. Intramolecular hydrogen bonding was assigned by adopting as geometric definition a distance between the two atoms H and Y less than 0.24 nm and a X−H···Y angle greater than 150°.

Definition of Parameters. The actual sequence of the two comonomers in the several oligomers is always represented by starting with an uronic residue U as the nonreducing end and ending with an acetylglucosamine residue A as the reducing end, since the enzymatic digestion with hyaluronidase proceeds by hydrolysis of the (1→4) glycosidic linkage. This specificity simplifies the definition of the structure of the oligomers used here as $(UA)_n$, with $n = 2-6$. The index n indicates the degree of polymerization of the oligomeric fragment for which the resonances were determined**.** Assignments of the ^{13}C spectra run at 100 MHz of hyaluronan oligomers $(UA)_n$ were given on the basis of the available literature[28,29] and resonances were attributed to specific C_mA_i and C_mU_i carbons, where the index m refers to the position of the C atom in the ith *N*-acetylglucosamine residue (A) or glucuronate residue (U), respectively. Most of the definitions used here are consistent with those reported by Cowman et al.[18]

Results and Discussion

Experimental ^{13}C NMR Data. The 100 MHz ^{13}C spectra of the five oligomers $(UA)_{n=2,6}$ are shown in Figure 1. From these experimental data, the values of the chemical shifts and the NOEF, T_1, and T_2 were calculated for each carbon atom. The numerical values of these parameters are reported in Figure 2 for the ring carbon atoms of the tetrasaccharide $(UA)_2$ in the β form, while the insert shows the values for the α form of the terminal portion ending with A_2. Resonances of C1 of the oligomer reducing end, due to α, β anomeric forms, were detected and classified in terms of chemical shifts up to the pentamer (10 saccharidic units). All unreported experimental values are available upon request. Resonances relative to end terminal effects were not detected in the spectra carried out on the hexamer (12 saccharidic units). Before we analyze the average dynamic properties, two examples of changes of the spectral profiles of ^{13}C resonances as a function of n are reported below. This description allows us to focus on the validity of the interpretative frame early proposed by Cowman et al.[18] as well as on some deviations from this scheme for a few resonances.

Behavior of the C_2A_i System. The C_2A_i system of carbon atoms displays, in $(UA)_2$, one peak at 54.9 ppm

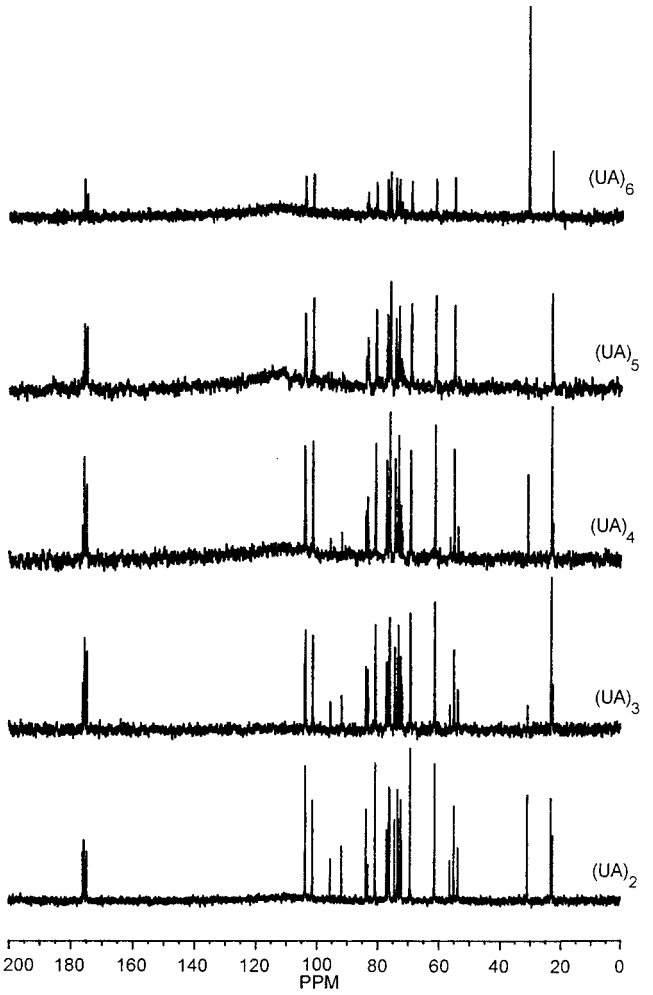

Figure 1. 100 MHz ^{13}C NMR spectra of the hyaluronan oligomers $(UA)_n$ ($n = 2-6$) in aqueous solution.

and two peaks of the reducing GlcNac residue at 53.5 and 56.2 for the α and the β anomers, respectively (Figure 3). The two peaks in $(UA)_3$, at 54.9 and 54.95 ppm, with relative intensities 1:1, are assigned to C_2A_1 and to C_2A_2, respectively. In $(UA)_4$ and $(UA)_5$ the relative intensities of the two peaks of the C_2A_i system with resonances at 55 ppm and at 55.05 ppm confirm the structural considerations previously proposed.[18] Analogous to the oligomer $(UA)_3$, the former is assigned to the penultimate residue (C_2A_1) carbon atom and the latter to the internal residues. Differences observed in the chemical shifts between penultimate and internal sugar residues are due to the distinct chemical environment relative to the external (penultimate residue) and internal β-1,3 linkage. A dynamic parameter such as NOEF qualitatively supports this interpretation, since in $(UA)_4$ the C_2A_1 signal of the penultimate A residue shows a value of 1, whereas the peak assigned to C_2A_2 and to the C_2A_3 carbons of the internal A residues have a NOEF of 0.8. This evidence shows that these chemical differences are coupled with differences in the dynamic behavior consisting of a stiffer conformational state of the internal residues with respect to the penultimate A unit.

Analogous behavior of the NOEF parameter is observed in $(UA)_5$ where a stiffening process occurs for the internal residues (NOEF: 0.93), while the penultimate A residue is comparatively more flexible (NOEF: 1.5). In $(UA)_6$, (not shown), only a peak at 55 ppm is present

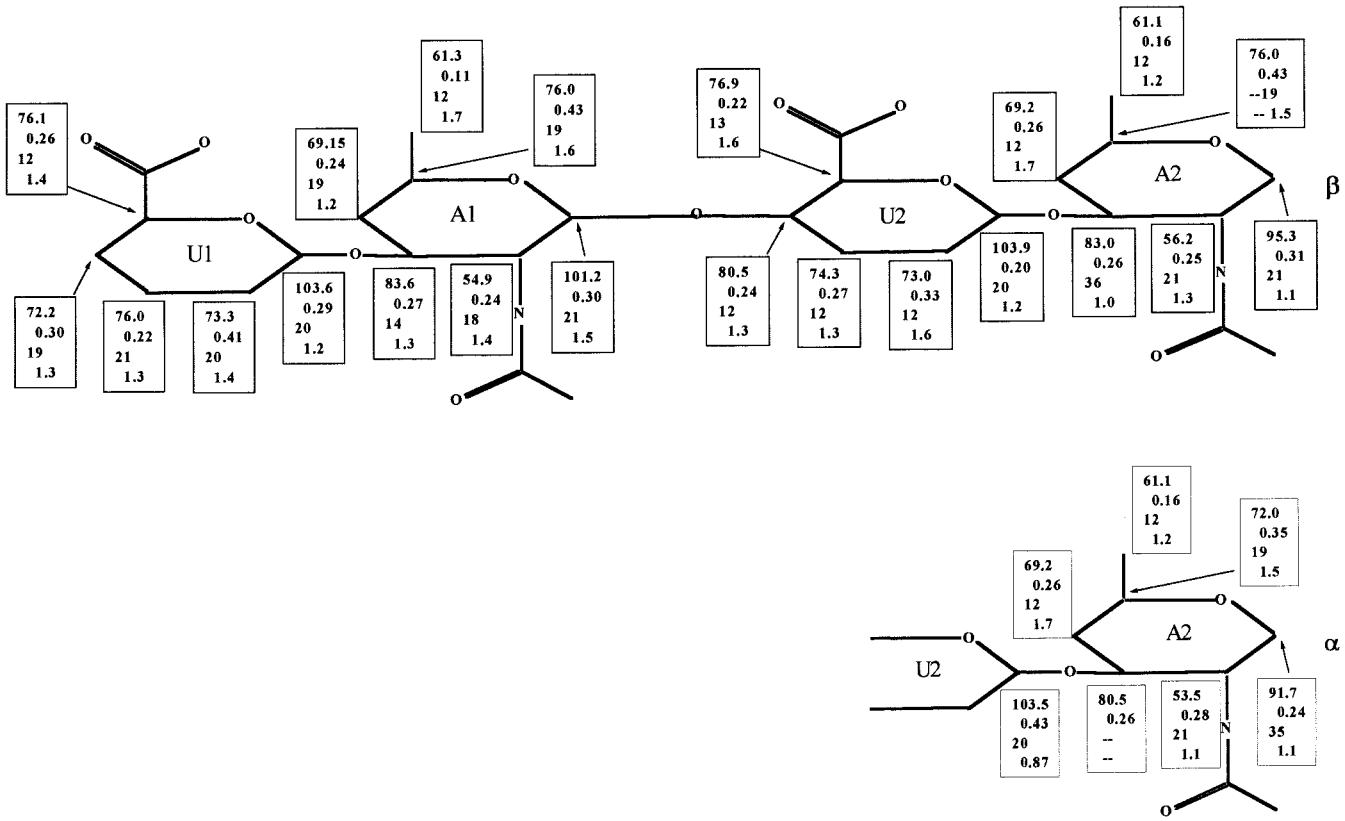

Figure 2. Schematic representation of the hyaluronan dimer $(UA)_2$ with the NMR data. The four digits in each column are the values of chemical shift (ppm), T_1 (s), T_2 (ms), and NOEF. The values of the chemical shifts of C_4 of A units have been rounded-off (see text and Figure 4). The insert (bottom) shows the values obtained for the α-form of the terminal A unit.

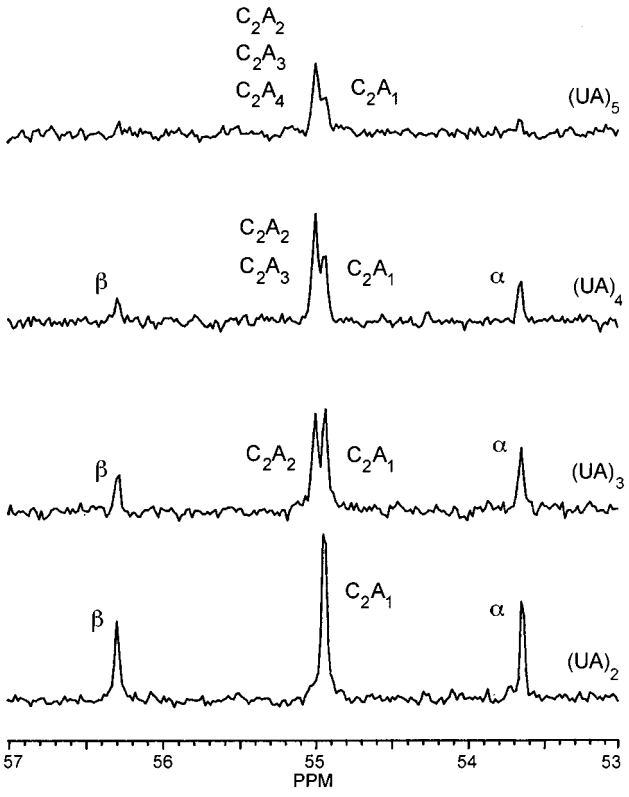

Figure 3. Behavior of peak resonances of the carbon atoms C_2A_i of the nonreducing end unit (A_1) and of the internal units (A_2−A_4). Resonances of C_2 of the anomeric forms at the reducind end are also included.

with a NOEF value of 0.77, indicating an increasing stiffening in the hexamer and a simultaneous disappearing of the penultimate residue C_2A_1 carbon, since end groups were not detectable at this *n* value.

Behavior of the C_4A_i System. The peak evolution as a function of *n* of the C_4A_i system can also be interpreted in terms of the relative position of the A sugar residues along the chains with different degrees of polymerization. In the dimer $(UA)_2$ we observed a peak at 69.1 ppm (NOEF value: 1.2) with a shoulder at 69.15 ppm (Figure 4). The individual assignment of these resonances is not possible since the peaks reflect a specific magnetic environment due to either different chemical or conformational states which, at present, cannot be assigned univocally. In $(UA)_3$ the C_4A_i system the shoulder present in the dimer spectrum evolves to a peak that forms with the resonance at 69.1 ppm a doublet whose relative intensities are approximately in the ratio 2:1. The two signals develop into a doublet in the tetramer (octasaccharide), whereas in the pentamer $(UA)_5$ the pattern of the intensities reverts to that of the $(UA)_2$ and $(UA)_3$ cases. Using the above-mentioned interpretative frame,[18] we can assign the peak envelope of the dimer to a partial overlapping of the resonances pertaining to the penultimate and terminal A units. In $(UA)_3$ the grouping of the terminal and penultimate acetamido sugars, separated from the peak of the internal A unit, results in the 2:1 intensity ratio. As the length of the oligomers increases, so does the intensity of the peak at 69.0 ppm, corresponding to the increasing number of internal units. Because of this effect, in the case of $(UA)_4$, a doublet is generated with intensities in the ratio of nearly 1:1, i.e., the number of internal A's being equal to the terminal and penultimate units. In the case of the pentamer, we observed a further increase in the peak relative to the internal units

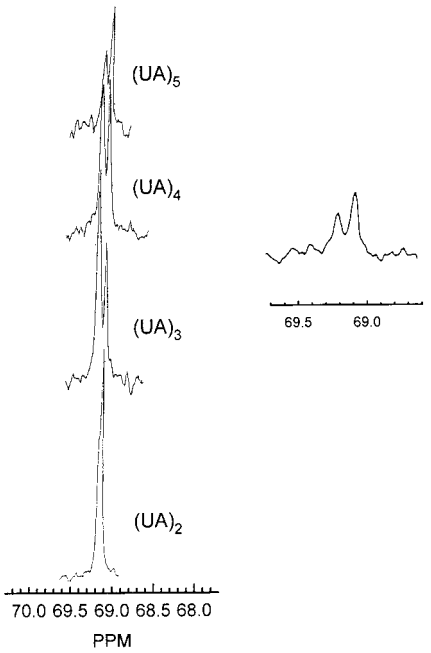

Figure 4. Behavior of peak resonances of the carbon atoms C_4A_i. Insert: C_4A_i for $(AU)_6$.

(69.0 ppm), i.e., the number of internal A units being three.

Although this analysis offers a successful explanation for the behavior of C_4A_i, C_2A_i, and similar systems, a caveat must be made since the behavior of C_4A_i carbons in $(UA)_6$ cannot be fitted into the above interpretation. The insert of Figure 4 is a close-up of the hexamer ^{13}C spectrum as far as the C_4A_i system is concerned and it shows that the two peaks, with comparable relative intensities, persist up to the dodecasaccharide chain. Even if the possible contamination of higher DP oligomers ($n > 6$) in the hexamer fraction is taken into account, the relative intensities of the peaks rule out the hypothesis that one of the resonances can be due to terminal effects. This result has been interpreted as evidence that additional effects, supposedly of the conformational type, may take place at or after $n = 6$. It has yet to be ascertained whether this conformational effect is related to the "second helical conformation" proposed for the same range of DP by the theoretical results reported by Almond et al.[30] As supporting evidence for the presence of structural motifs, the average NOEF of internal A and U sugar residues shows a sort of progressive "stiffening" of the chain which continues also in the hexamer. However, it must be specified that here the term "stiffening" has been (and is often) used to underline changes in the static and dynamic chain parameters, that obviously are also a function of the progressive increasing anisotropy of the cylindrically shaped chain segments. Presently, we cannot be certain as to whether the dynamic result is an effective probe of the internal motion, or major changes occur for mere dimensional effects. These findings are qualitatively in agreement with those reported by Cowman et al.,[38] although the different averaging methods used in this paper have to be considered.

Experimental Averaged Dynamic Properties. Dipole ^{13}C relaxation parameters NOEF are relevant to the understanding of the local dynamic behavior of a sugar residue in an oligomer chain in solution. The overall trend of NOEF, T_1, and T_2 has been evaluated

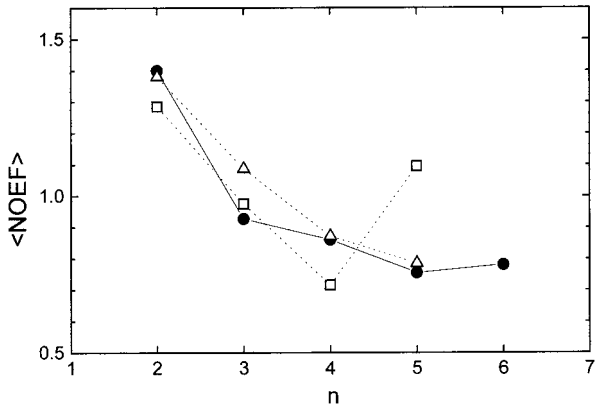

Figure 5. Chain-length dependence of NOEF values averaged over the ring carbon atoms (C1−C5) of the internal A and U residues (●), over the carbon atoms of the nonreducing U end (□) and of reducing A end (Δ).

as a function of the increasing size of the chain segment by averaging the values of these parameters over the five ring carbons for the glucuronate (U) and the *N*-acetylglucosamine (A) residues, respectively. This approach had already been used by several authors[29,31] in the case of the high molecular weight polymer. As a general trend, the average value of ⟨NOEF⟩ decreases with increasing degree of polymerization, *n*, for both A and U residues, indicating a progressive dynamic slowdown of the chain as its size increases (Figure 5). From these data, although some irregularities seem to occur in the trend for the A residues passing from $n = 4$ to $n = 5$ and 6, consistent behavior is seen for the dynamic properties in terms of NOEF of moieties having the same (or even only similar) chemical nature. The similarity of the trends of both moieties confirms a strong dynamic correlation between the residues, irrespective of their chemical diversity. A comparison of the dynamic behavior of the two terminal residues, the reducing A and the nonreducing U, respectively, is shown in Figure 5. The size-dependent hampering of the hyaluronan oligomers is evident with a substantial agreement of the values of NOEF for both ends, besides the anomaly observed for the reducing end (A) of the pentamer, which is outside the experimental error.

Comparison of the T_1 parameters of the nonreducing end with those of the internal glucuronic residues is noteworthy since it illustrates the influence of the chain length, *n*, on the behavior of this NMR dynamic parameter. Similar values and trends are observed for both types of residues, analogous to what has already been found in the NOEF data. The results shown in Figure 6 indicate some higher mobility of the nonreducing end with respect to the internal uronic residues only for the first two oligomers ($n = 2$ and 3). In fact $\langle T_1 \rangle$ increases with decreasing rate of motion in this specific dynamic regime. The behavior of T_1 of the uronic moieties seems to level off to about the same value for the higher molecular weight oligomers (DP 5 and 6). In Figure 7 the increasing T_1 average values of the reducing end and the internal A residues are reported as a function of *n*. Therefore, the decrease in mobility with the chain length *n* of the reducing terminal A seems to be larger than that of the nonreducing end residue U.

Before illustrating the dependence of the intensities detected for some carbon atoms as a function of the degree of polymerization, let us conclude that, from the "average" behavior of the residue, the dynamic proper-

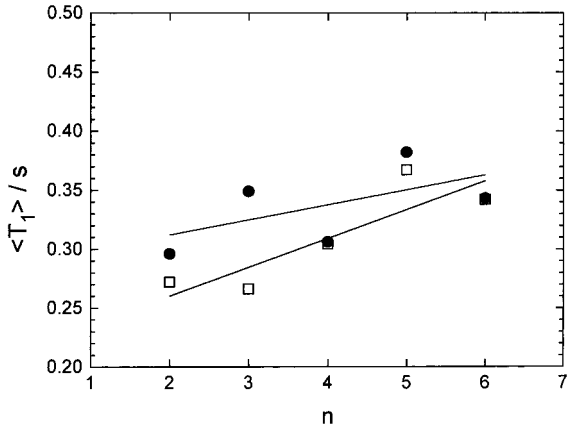

Figure 6. Average T_1 of carbon atoms of hyaluronan oligomers: internal U residues (●) and nonreducing U ends (□).

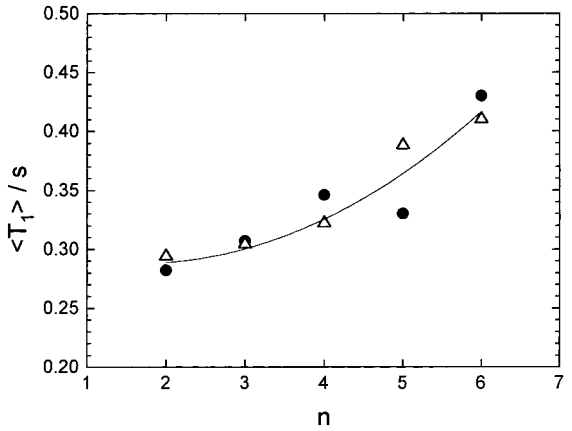

Figure 7. Average T_1 of carbon atoms of hyaluronan oligomers: internal A residues (●) and reducing A ends (Δ).

ties are consistent with an overall slower motion of the larger oligomers which, however, has not yet been resolved into the various local components.

The comparison between the residual $\langle T_1 \rangle_{res}$ values, obtained by averaging over the five carbon atoms of each A and U ring for the oligomers, reveals differences in internal mobility between the A and U units as a function of the position of the unit and of size of the oligomer. Figure 8 reports the behavior of these average quantities $\langle T_1 \rangle_{res}$ for the residues of the dimer, trimer and tetramer, respectively. For the tetrasaccharide $(UA)_2$ the $\langle T_1 \rangle_{res}$ values are nearly similar except for the lower value observed for the unit U2. The situation is apparently more complex for the hexasaccharide $(UA)_3$. It can, however, be rationalized by splitting the segment into two parts: the three A units maintain approximately the same mobility, while the U rings increase their mobility from the reducing end to the nonreducing end. This gives the characteristic zigzag pattern from the reducing end. No explanation can be given at the moment for the inversion of pattern presented by the octamer $(UA)_4$, which apparently contradicts the interpretation conceived for the two shorter oligomers (Figure 8C). As a preliminary speculation, it may only be supposed that the topology of the pseudo-helical segment imposes a different distribution on the dynamic pattern, indicating that a different regime should be observed in the HA chain.

Internal Motions from Individual Relaxation Data. An analysis of T_1 and NOEF values of the ring carbon atoms along the chain has been carried out by

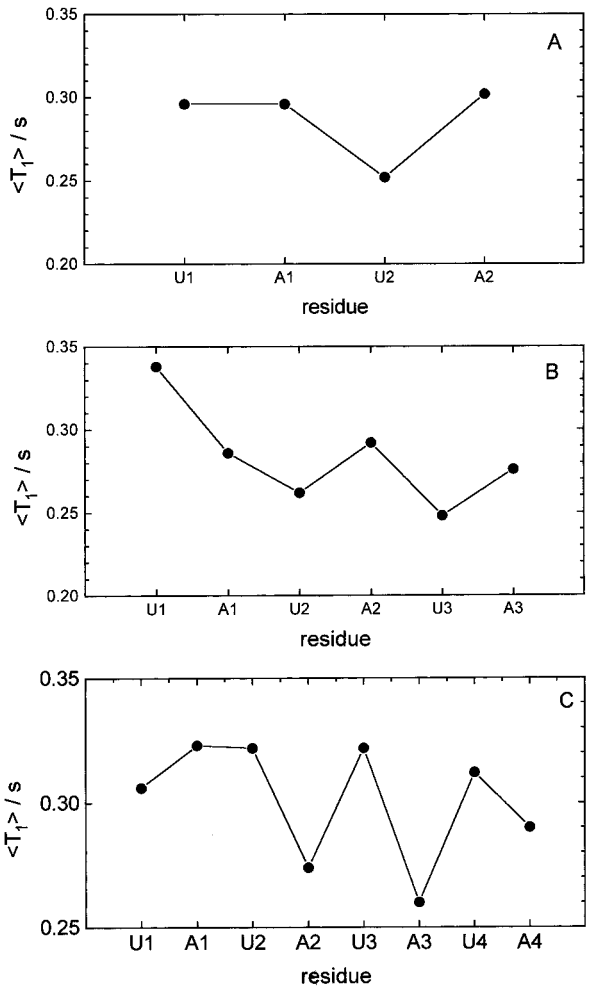

Figure 8. Longitudinal relaxation time values, T_1, averaged on each U and A residues for the dimer (A), trimer (B), and tetramer (C), respectively.

means of the "Model Free Approach", proposed by Lipari and Szabo[32,33] for the determination of the internal fast motions in macromolecules from the relaxation data at one magnetic field. A multifrequency approach would have been more informative for the study of local motions in a polymer chain, but at this stage the goal was mainly to compare the local dynamic behavior along the segment for each oligomers. The values of the effective correlation times of internal motion obtained by the procedure reported in ref 32 were all faster than the overall tumbling motions. Thus, the "effective" values of the angle of wobbling in a cone for the individual CH bonds have been evaluated considering an overall correlation time as obtained by the direct application of the Stokes rigid body rotation. The analysis is limited to the CH of the carbons belonging to the saccharide rings, as calculations showed that the values found lies in the minimum of the T_1 vs correlation time curve (data not shown). Other more detailed formalisms with adjustable parameters (accounting for anisotropic motion and chemical shift anisotropy relaxation mechanism) were not considered appropriate for the data here reported.

By using the Model Free Approach with the relaxation time T_1 and the NOEF of the resolved resonances attributed to individual carbon atoms of the oligomeric chains, the calculation gives the frequency of motion as the inverse of the effective correlation time and of the

order parameter S^2, and therefore the angle θ of the motion described by the CH dipole. This is just as before, only the relaxation data of carbon atoms of the ring are included and not the carbon atoms of the methylene groups.

The scrutiny of the θ values indicates that, although some absolute values may appear excessive for fast motions overposed to a slow motion, their differences along the sequence from one end to the other show clearly a positional dependence of the local motion.

For a suitable description and comparison of internal motions of the different molecular regions of chains with different lengths, the presentation of the results has been sorted by dividing the "ribbonlike" pseudo-helical chain into two sides,[17] one being called "up" and the other "down". This geometrical separation corresponds to topological considerations, although it may not fully correspond to the chemical periodicity of the carbon atoms along the saccharidic sequence. To show the effect of the position of individual carbon atoms the θ angle related to the local mobility of the chain are reported in Figures 9−11, for $(UA)_2$, $(UA)_4$, and $(UA)_4$, respectively, aligning the sequence of the carbon atoms at the "up" (A) and "down" (B) sides of the chain.

Inspection of θ values for $(UA)_n$ indicates that the internal flexibility is not uniformly distributed within the individual oligomeric units as indicated by the difference in T_1 and NOEF values. Overall, a sort of complementarity in flexibility is present in the units. When one side of the oligomeric chain appears more flexible the other is more stiffened. In the case of $(UA)_2$ it is clear that when a large oscillation of the CH dipole indicated by θ values is present in one side (e.g., "up") of the molecule then, as counterbalance, a stiffening occurs with a concurrent reduction of mobility on the other side ("down"). For example, the θ values at the reducing end (right) in the A_2 of $(UA)_2$ (Figure 9) indicate that C1, C2, and C3 carbon atoms are hampered (low θ values) while C4 and C5 carbon atoms are more mobile (high θ values). The same trends are also visible in Figure 10 for $(UA)_3$ and in Figure 11 for $(UA)_4$. In the latter a marked reduction in flexibility at the junction between A and U units is clearly noticeable. It should also be noted that an overall comparison between the values in $(UA)_2$ and $(UA)_4$ led to the observation that in the latter, a very high number of stiffened junctions is present, particularly at C3 and C4 of internal A and C5 of internal U units while the very flexible carbons are the C1 carbons of the U units.

In the above results, it is important to note that by increasing the length of the oligomers a high flexibility is located around the C1 of both U and A. Therefore, if stiffening is generated by shared hydrogen bonds, this produces only a partial stiffening effect on the remaining units. Some hypotheses can be borne out regarding the crucial role of the hydrogen bonds distributed along the units of the oligomeric chains. Few "in-registry" hydrogen bonds introduce a stiffening effect and rigidity. A series of hydrogen bonds distributed randomly, and probably mutually excluding each other in dynamic equilibrium, has the effect of averaging the motion along the chain by introducing some flexibility homogeneously stepwise distributed, rather than a localized strong stiffening between the two UA monomers.

Molecular Dynamics Simulations. The behavior of two hyaluronan fragments, i.e., a dimer and a tetramer, has been explored up to 700 ps, bearing in mind the dynamic NMR set of data already collected. Both molecular fragments were built consistent with the enzymatic cleavage obtained in the fractions investigated by ^{13}C NMR; i.e., the nonreducing end is a U residue while the reducing end consists of an A unit. The β anomeric form was assigned to the reducing end, as had already been done in dynamic simulations in the literature.[30] Only a preliminary evaluation of some outputs of the conformational dynamics of hyaluronan is reported here to provide a qualitative comparison with experimental findings. More extensive simulations on several hyaluronan fragments in aqueous solution are presently being undertaken and will be discussed at a later date in a separate work.

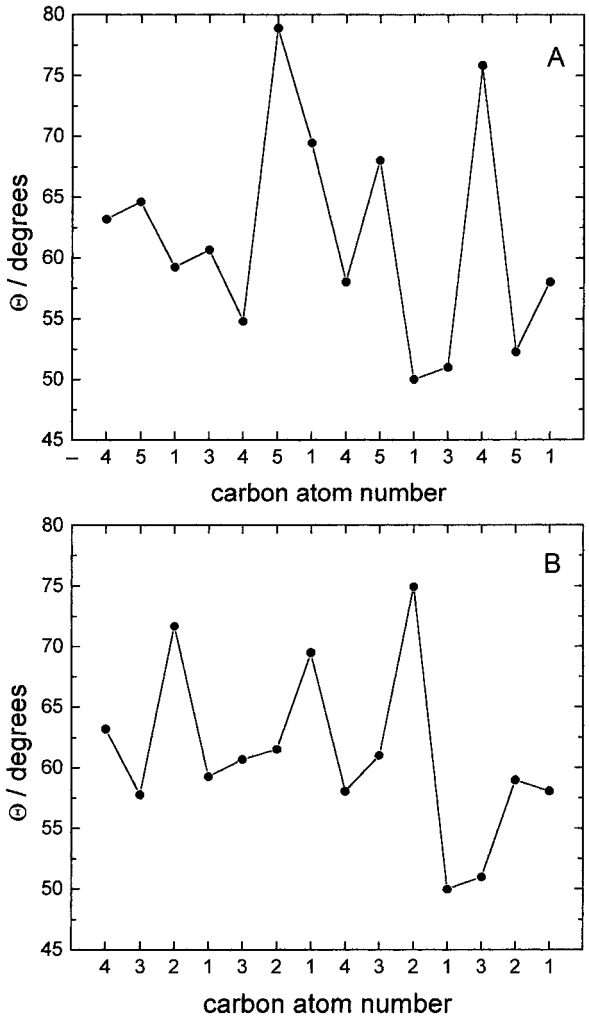

Figure 9. Fluctuation of Θ parameter (see text) as a function of the carbon position in the $(UA)_2$ for the edge "up" (A) and for the edge "down" (B), respectively.

Dynamics Simulation of Dimer, $(UA)_2$, and of Tetramer, $(UA)_4$. Simulations over a period of 700 ps were mainly focused on the variations of the glycosidic linkage torsion angles and on the persistence of intramolecular hydrogen bonds. Figure 12 reports the time evolution of the three glycosidic dihedral angles ϕ_i, ψ_i; Table 1 reports their mean values and root-mean-square (rms) fluctuations for the trajectory. A distinctive feature of the (1→3) glycosidic linkages is the exploration of a fairly broad region of the conformational space (with a deviation of up to ±20° for both angles ϕ_i, ψ_i), though within the same potential energy well reported in the Ramachandran-like energy maps of the corre-

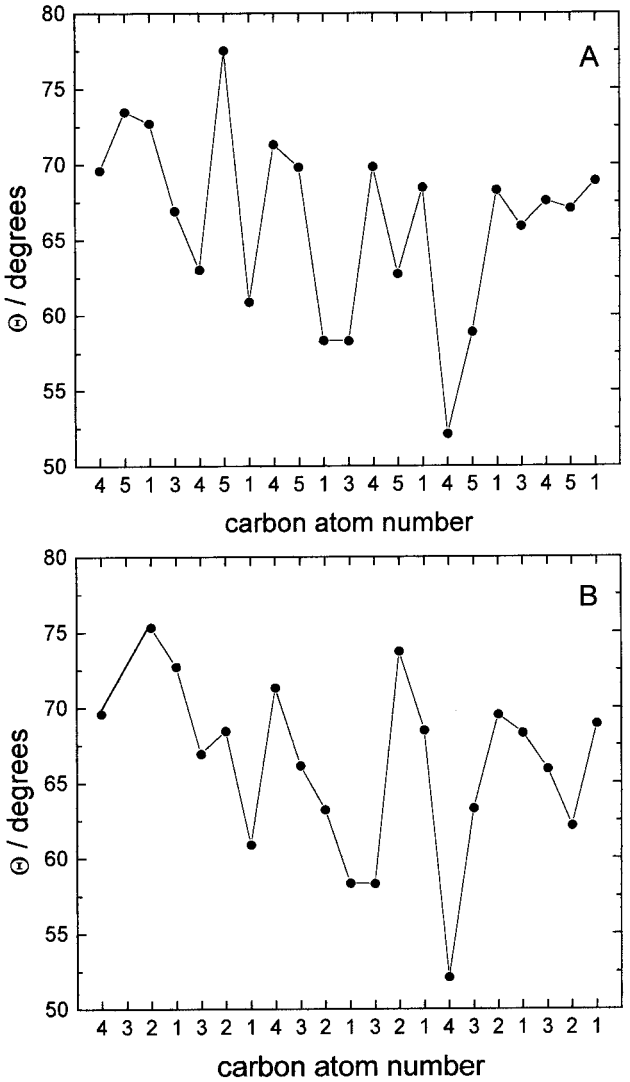

Figure 10. Fluctuation of Θ parameter as a function of the carbon position in the $(UA)_3$ for the edge "up" (A) and for the edge "down" (B), respectively.

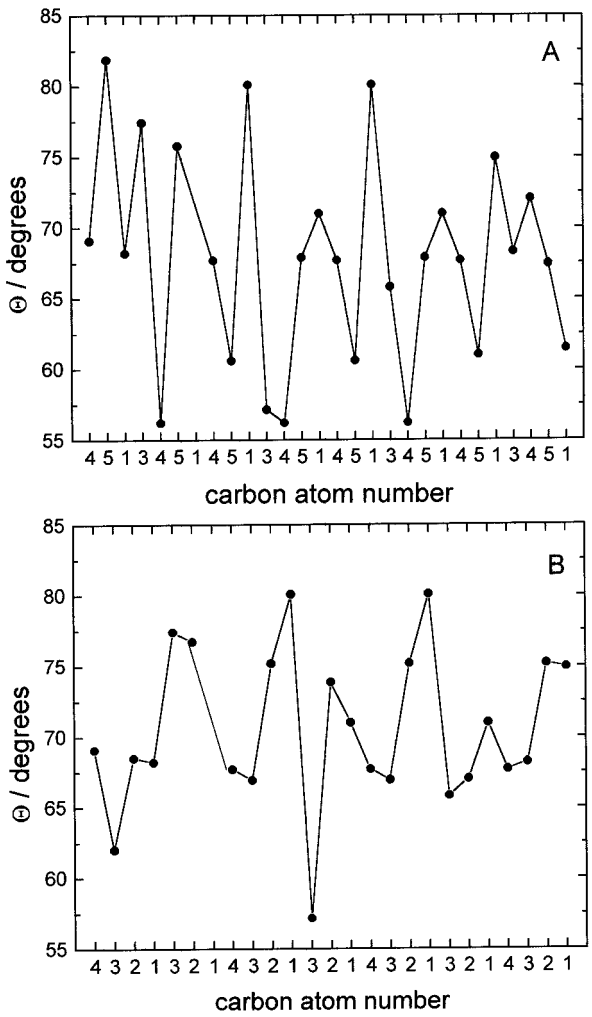

Figure 11. Fluctuation of Θ parameter as a function of the carbon position in the $(UA)_4$ for the edge "up" (A) and for the edge "down" (B), respectively.

sponding monomer.[34] In addition to oscillations in the main minimum, the (1→4) linkage undergoes a transition at about 160−300 ps, also populating a second conformational region. This difference in flexibility between the (1→3) and (1→4) linkages is in agreement with the results of Holmbeck et al.[35] obtained by means of a statistical solvation model.[36] On the contrary, the simulation of the two tetrasaccharides of hyaluronan, $(UA)_2$ and $(AU)_2$, in solution[16] predicts a tight constraint of the central linkage (ϕ_2, ψ_2) for both molecules giving rise to a single conformation irrespective of the type of linkage. The resulting conformation of Almond et al.[16] is in agreement with one of the two found in these simulations carried out in vacuo.

A correlation between the accessible conformational states and the intramolecular hydrogen bonding for the dimeric molecule has been found in the trajectories. The pattern of the most probable intramolecular hydrogen bonds and the probability (percentage) of a particular hydrogen bond are also reported in Table 1. The hydrogen-bonding network along the $(UA)_2$ molecule involves the ring oxygen (O5), as hydrogen acceptor, and the O4 or O3 for (1→3) or (1→4) linkages, respectively, of the following sugar, as hydrogen donor. A second pattern of hydrogen bonds implies the *N*-acetylamino group as linker between adjacent sugars. However, it should be mentioned that the data in Table 1 do not stress that H-bonds may not be formed all together and at the same time but that they do compete with each other. Figure 13 shows an example of correlation between conformational space and potential hydrogen bond formation for the tetrasaccharide, referring to the code used in Table 1. In general, the hydrogen bonds across the (1→4) linkage are less stable than those

Table 1. Ensemble-Averaged Mean Values and Fluctuations for ϕ and ψ Glycosidic Dihedral Angles and Probability of the Intramolecular Hybrogen Bonds for $(UA)_2$

glycosidic linkage	dihedral angle[a]	mean	rms fluct	H-bond[b]	prob, %
(1→3)[c]	ϕ_1	41	9	$O_5U_1-O_4A_1$ (a)	21
(U_1→A_1→)	ψ_1	6	14	$O_2U_1-O_7A_1$ (b)	45
(1→4)	ϕ_2	43; −55	11; 11	$O_5A_1-O_3U_2$ (c)	19
(→A_1→U_2→)	ψ_2	−3; −48	13; 10		
(1→3)[d]	ϕ_3	37	11	$O_5U_2-O_4A_2$ (d)	18
(→U_2→A_2)	ψ_3	2	13	$O_2U_2-O_7A_2$ (e)	12

[a] Increasing numbering of dihedral angles is from the nonreducing end of the sugar. Odd and even numbers refer to (1→3) and (1→4) glycosidic linkages, respectively. [b] Only the hydrogen bonds with probability greater or equal to 1% are reported. The H-bonds are identified by the oxygen atoms number and the sugar unit (letters refer to Figure 13). [c] Nonreducing end. [d] Reducing end.

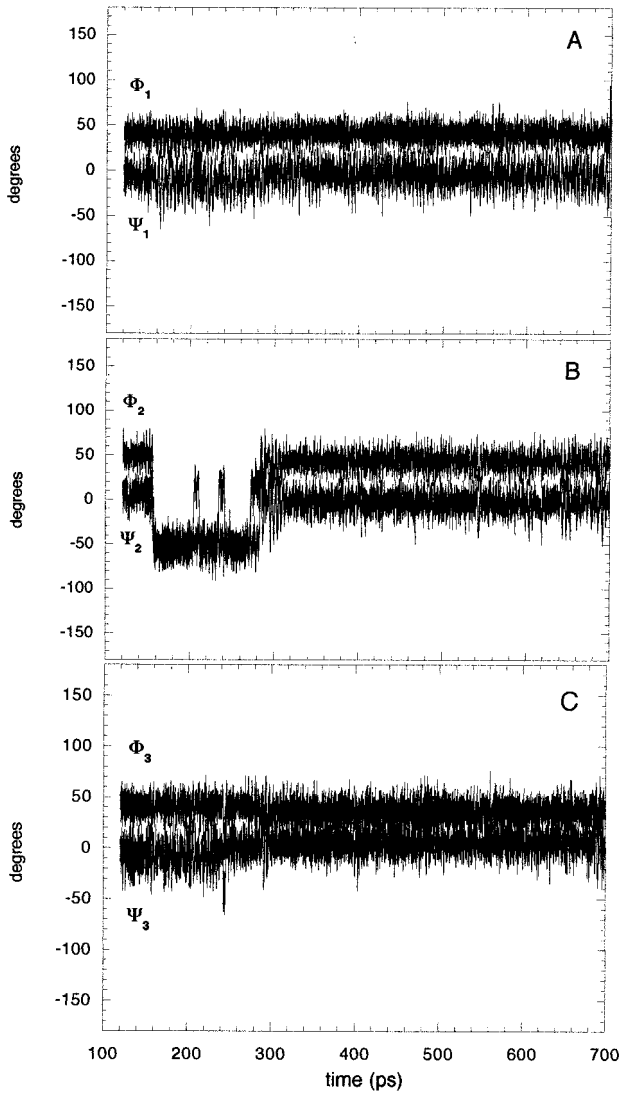

Figure 12. Time evolutions of the three glycosidic dihedral angles ϕ_i, ψ_i for the dimer $(UA)_2$. See also entries 1−4 in Table 1.

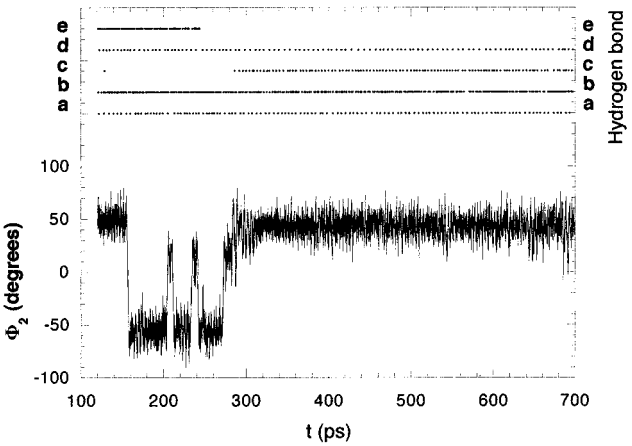

Figure 13. Correlation between conformational fluctuation and hydrogen bond formation for the glycosidic linkages of the dimer $(UA)_2$. See also entries 5−6 of Table 1.

across the (1→3) linkage due to the geometry of the oligosaccharidic chain. However, it is the alternative hydrogen bond around this glycosidic link that can stabilize the second conformational state. Because of different end effects, some differences are found between

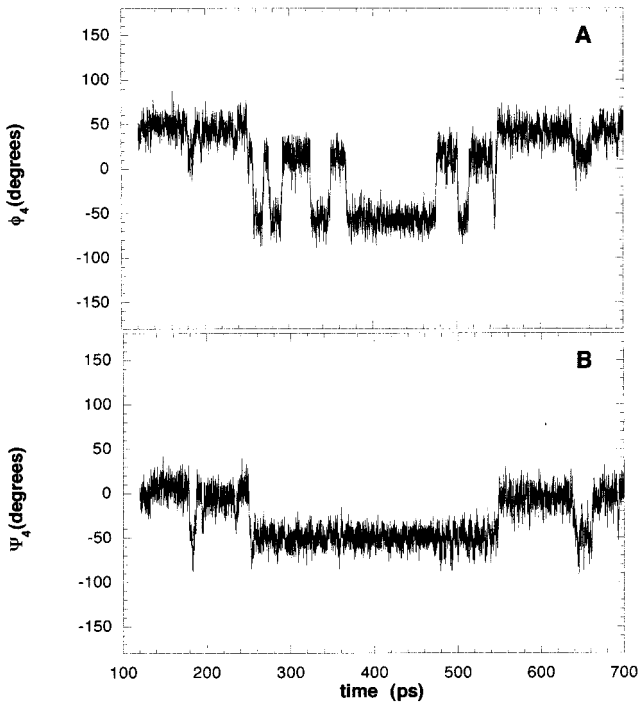

Figure 14. History of (ϕ_4, ψ_4) dihedral angles, related to the A_2-U_3 linkage of tetramer $(UA)_4$.

the two (1→3) linkages, since the same hydrogen bond pattern cannot be reproduced in both cases. In fact, the orientation of the acetamido group at the reducing end is poorly defined due to the lack of a neighboring carboxylic group. Therefore, time fluctuations of ϕ_3 and ψ_3 are different from those of the ϕ_1, ψ_1 pair. A comment is necessary on the evolution of these hydrogen bonds in oligosaccharides surrounded by water molecules. In general, it is expected that intraresidue hydrogen bonds would be easily broken if the hydroxyl groups involved could make alternate bonds with water molecules. Preliminary studies in progress reveal minor effects on the overall conformational states, although the analysis of the water density around the polar and nonpolar groups of the molecule can give much more insight on the actual solvation of the hydrophilic groups in these systems. For example, it has been surprisingly demonstrated by Brady and others on small sugars[37] that probability density supports an "ambiguous" position of water molecules between two adjacent sites, more than a "jumping" between the two otherwise conceivable minima for net hydrogen bondings.

The simulations have been extended to a $(UA)_4$ fragment. The time series of the glycosidic linkage torsion angles of the octasaccharide, seven (ϕ ,ψ) pairs, show that the (1→3) linkages are less flexible than the (1→4) linkages, as found for $(UA)_4$. One or two conformers are populated for the (1→3) and at least three for the (1→4) linkages. Figure 14 shows the history of (ϕ_4, ψ_4) dihedral angles, related to the middle linkage of the oligosaccharide, as an example. The results show that a lower mean lifetime seems to be associated with each conformational state, in comparison to that obtained for $(UA)_2$. The mean probability of hydrogen bonding is lower than the corresponding one for the tetrasaccharide, which seems to be related to higher conformational freedom. As shown in Table 2, the dihedral angle pairs have root-mean-square fluctuations greater than those found in the dimer case. These results, although only

Table 2. Ensemble-Averaged Mean Values and Rms Fluctuations for ϕ_i and ψ_i Glycosidic Dihedral Angles of $(UA)_4$[a]

dihedral angle[b]	1	2	3	4	5	6	7
ϕ_i	41 (9)	−1 (36)	35 (19)	12 (42)	21 (30)	29 (33)	35 (19)
ψ_i	−8 (13)	−44 (18)	−11 (15)	−25 (26)	−15 (14)	−25 (28)	−8 (15)

[a] Rms fluctuations are given in parentheses. [b] Increasing numbering of dihedral angles is from the nonreducing end of the sugar. Odd and even numbers refer to (1→3) and (1→4) glycosidic linkages, respectively.

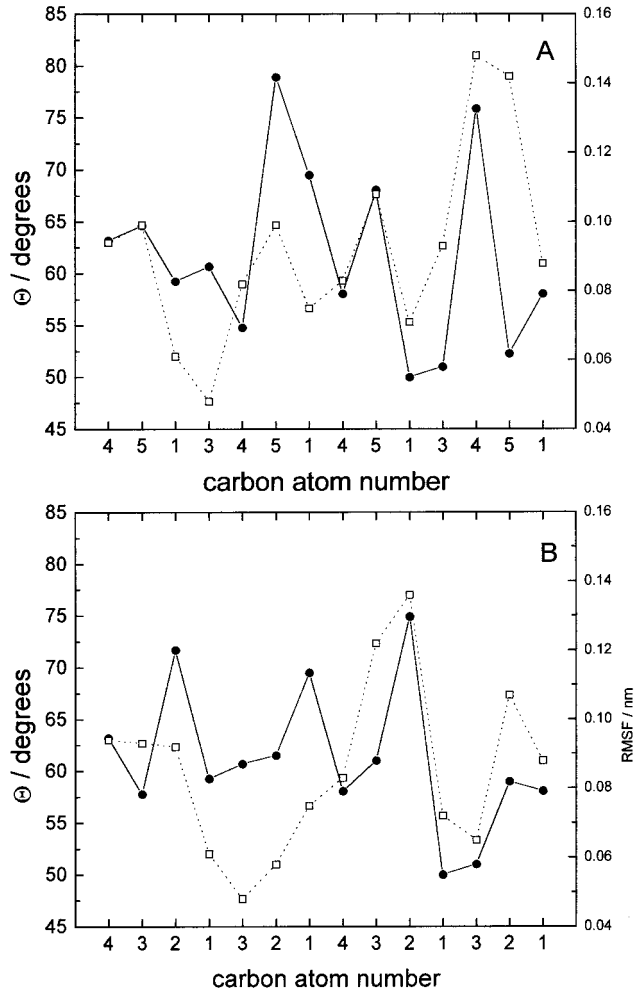

Figure 15. Comparison of the Θ parameter (●) with the RMSF values (□) calculated from the trajectories of the simulations for the dimer $(UA)_2$: (A) edge "up"; (B) edge "down".

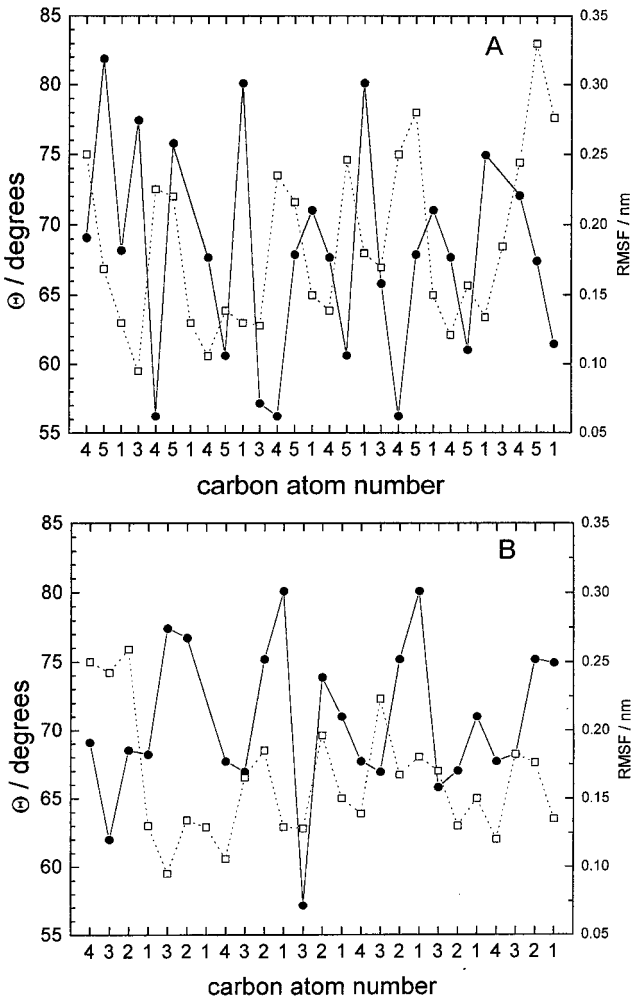

Figure 16. Comparison of the Θ parameter (●) with the RMSF values (□) calculated from the trajectories of the simulations for the tetramer $(UA)_4$: (A) edge "up"; (B) edge "down".

preliminary and restricted to "in vacuo" conditions, are reported here for two main reasons. First, it seems that the behavior of HA polymer can be fully understood only if the progressive changes in the properties of oligomers are explored. Second, the simulations can be used here to correlate the model-calculated rms with some significative experimental dynamic data, as illustrated in the following section.

Comparison of Experiments and Simulations. To obtain some relationships between the individual relaxation data and the internal flexibility a comparison has been made between the θ values and the root-mean square fluctuations (RMSF) of the hydrogen atom of the CH bonds during the molecular dynamics simulation. This comparison is reported in Figure 15 and 16 for $(UA)_2$ and $(UA)_4$, A and B indicating the "up" carbons and the "down" carbons, respectively. For the $(UA)_2$ a surprisingly good correlation was obtained between the θ values obtained from ^{13}C relaxation data and the RMSF calculated from the trajectories of the simulations. A poorer correlation is found for the same comparison between the NMR results and the RMSF of the simulation reported in Figure 15. While the central region of the oligomer shows a certain similarity in the θ and RMSF values in the simulations, two well-defined lateral regions show a marked discrepancy between the experimental and simulated data. In this case, the simulation overestimates the stiffening introduced probably as a result of an over-extensive hydrogen bond regime with respect to reality. In other words, the oligomers show an internal mobility higher than that expected in the simulations where probably, changes of dynamic behavior of the intramolecular hydrogen bond regime have not been properly taken into account.

Final Remarks

From the structural point of view, high molecular weight hyaluronan dynamics can be envisaged as

depending mainly on the following factors: alternating (1→3) and (1→4) glycosidic bonds with different flexibility, water molecules clustered in different domains of the chain, and hydrogen bonding enhancing intramolecular connectivity. All these aspects put hyaluronan in the class of complex molecules for modeling in terms of dynamics simulation. Literature data and dynamics simulation for some polysaccharides, like pullulan and amylose oligomers, show a leveling off in their dynamic behavior when passing from simple oligomers to high molecular weight polymers.[19] In general, a critical degree of polymerization is reached above which the segmental mobility of the high molecular weight polymers is matched (for flexible polymers, usually with $n > 20$). More elongated chains, like cellulose and galactans, go in exactly the opposite direction and decrease their internal mobility with increasing molecular weight, thus diverging from the asymptotic behavior. Given the copolymeric character of HA, it is expected that the coupling of two junctions with different rotational freedom can affect the trend of the dynamic pattern of higher oligomers, the β-1,3 linkage belonging to the first class and the β-1,4 linkage to the second class of polymers. A proper combination of experimental dynamic data with model calculation has been considered useful in rationalizing the solution behavior of HA. Unfortunately, none of the dynamic models developed for the description of relaxation motion in oligomeric and polymeric systems is directly based on the peculiar ring-shaped geometry of polysaccharide structure; nonetheless, the availability of detailed experimental NMR dynamic parameters prompts the use of molecular dynamics calculations in an attempt to understand the behavior of these polysaccharide oligomers at molecular level. The approximation has been made here for the evaluation of possible modes of reorientation in a carbohydrate chain based on the "Model Free Approach" of Lipari and Szabo.[32,33] Specifically, we stress that the analysis carried out has been useful to extract some local dynamics information (although still qualitative) for comparison with the dynamics simulations and compares well with the results presented in the adjacent work by M. Cowman and co-workers.[38] A more extensive analysis of conformational dynamics of these systems seems to be necessary, however, before the results can be extended to describing the actual behavior of the high molecular weight polymer. In particular, the task is that of satisfactorily describing the segmental motion of each polysaccharide in solution, a problem which is far from being solved.[39] The primary need is for a TCF formulation, which can be accounted for explicitly by the geometric constraints of a carbohydrate chain in terms of its conformational space. By following this route, we aim to combine the present results with those that can be obtained through the diffusive theoretical approaches recently used for simple polysaccharides.[19]

Acknowledgment. The authors wish to thank A. Perico and M. Cowman for helpful discussions and J. R. Ruggiero and S. Letardi for some dynamic simulations. Financial support has been provided by the Progetto Coordinato "*Proprietà dinamiche di oligo e polisaccaridi*", Grant CT97-02765.03, and by the target project "Biotecnologie" of the National Research Council of Italy (Rome) and in part by the National Research Project (PRIN) "Biologia Strutturale" of Ministero della Universitá e Ricerca Scientifica e Tecnologica (MURST).

References and Notes

(1) Lapacik, L. Jr.; Lapacik, L.; De Smedt, S.; Demeester, J. *Chem. Rev.* **1998**, *98*, 2663−2684.
(2) Laurent, T. C. *The Chemistry, Biology and Medical Applications of Hyaluronan and its Derivatives*; Portland Press: London, 1998.
(3) Cleland, R. L. *Biopolymers* **1968**, *6*, 1519−1529.
(4) Cleland, R. L. *Arch. Biochem. Biophys.* **1977**, *180*, 57−68.
(5) Cleland, R. L. *Biopolymers* **1984**, *23*, 647−666.
(6) Hayashi, K.; Tsutsumi, K.; Nakajima, F.; Norisuye, T.; Teramoto, A. *Macromolecules* **1995**, *28*, 3824−3830.
(7) Morris, E. R.; Rees, D. A.; Welsh, E. J. *J. Mol. Biol.* **1980**, *138*, 383−400.
(8) Chakrabarti, B.; *Arch. Biochem. Biophys.* **1977**, *180*, 146−150.
(9) Gibbs, D. A.; Merrill, E. W.; Smith, K. A.; Balasz, E. A. *Biopolymers* **1968**, *6*, 777−791.
(10) Rao, V. S. R.; Qasba, P. K.; Balaji, P. V.; Chandrasekaran, R. *Conformation of Carbohydrates*; Harwood Academic Publ.: Amsterdam, 1998; Chapter 8, pp 258−263 and references therein.
(11) Scott, J. E. *The Biology of Hyaluronan*; Ciba Foundation Symposium 143; Wiley: Chichester, U.K., 1989; pp 6−20.
(12) Turner, L. R.; Lin, P.; Cowman, M. K. *Arch. Biochem. Biophys.* **1988**, *265*, 484−495.
(13) Manning, G. S.; *J. Chem. Phys.* **1980**, *51*, 924−933.
(14) Reed, C. E.; Li, X.; Reed, W. F. *Biopolymers* **1989**, *28*, 1981−2000.
(15) Ghosh, S.; Li X.; Reed, C. E.; Reed, W. F. *Biopolymers* **1990**, *30*, 1101−1112.
(16) Almond. A.; Brass, A.; Sheehan, J. K. *Glycobiology* **1998**, *8*, 973−980.
(17) Scott, J. E.; Heatley, F. *Proc. Natl. Acad. Sci. U.S.A.* **1999**, *96*, 4850−4855.
(18) Cowman, M. K.; Hittner, D. M.; Feder-Davis, J. *Macromolecules* **1996**, *29*, 2894−2902.
(19) (a) Perico, A.; Mormino, M.; Urbani, R.; Cesàro, A.; Tylianakis, E.; Dais, P.; Brant, D. A. *Phys. Chem. B* **1999**, *103*, 8162−8171. (b) Perico, A.; Mormino, M.; Urbani, R.; Cesàro, A.; Tylianakis, E.; Dais, P.; Brant, D. A. To be published.
(20) Martin, M. L.; Delpuech, J.-J.; Martin, G.; *Practical NMR Spectroscopy*; Heyden: London, 1980; p 231 and references therein.
(21) Brooks, B. R.; Bruccolieri, R. E.; Olafson, B. D.; States, D. J.; Swaminathan, S.; Karplus, M. *J. Comput. Chem.* **1983**, *4*, 187−217.
(22) Ueda, K.; Brady, J. W. *Biopolymers* **1996**, *38*, 461−469.
(23) Brady, J. W.; Schmidt, R. K. *J. Phys. Chem.* **1993**, *97*, 958−966.
(24) Smith, P. J. C.; Arnott, S. *Acta Crystallogr., Sect. A* **1978**, *34*, 3−9.
(25) Verlet, L. *Phys. Rev.* **1967**, *159*, 98−103.
(26) van Gusteren, W. F.; Berendsen, H. J. C. *Mol. Phys.* **1977**, *34*, 1311−1327.
(27) Stella, L.; Melchionna, S. *J. Chem. Phys.* **1998**, *109*, 10115−10117.
(28) Kvam, B. J.; Atzori, M.; Toffanin, R.; Paoletti, S.; Biviano, F. *Carbohydr. Res.* **1992**, *230*, 1−13.
(29) Hofman, H.; Schmut, O.; Sterk, H.; Pölzler, H. *Int. J. Biol. Macromol.* **1983**, *5*, 229−232.
(30) Almond, A.; Brass, A.; Sheehan, J. K. *J. Mol. Biol.* **1998**, *284*, 1425−1437.
(31) Benesi, A. J.; Brant, D. A. *Macromolecules* **1985**, *18*, 1109−1116.
(32) Lipari, G.; Szabo, A. *J. Am. Chem. Soc.* **1982**, *104*, 4546−4559.
(33) Lipari, G.; Szabo, A. *J. Am. Chem. Soc.* **1982**, *104*, 4559−4570.
(34) Almond, A.; Sheehan, J. K.; Brass, A. *Glycobiology* **1997**, *7*, 597−604.
(35) Holmbeck, S. M. A.; Petillo, P. A.; Lerner, L. A. *Biochemistry* **1994**, *33*, 3**,** 14246−14255.
(36) Still, W. C.; Tempczyk, A.; Hawley, R. C.; Hendrickson, T. *J. Am. Chem. Soc.* **1990**, *112*, 6127−6129.
(37) Liu, Q.; Schmidt, R. K.; Teo, B.; Karplus, P. A.; Brady, J. W. *J. Am. Chem. Soc.* **1997**, *119*, 9, 7851−7862. Liu, Q.; Brady, J. W. *J. Phys. Chem.* **1997**, *101*, 1317−1321.
(38) Cowman, M. K.; Feder-Davis; J.; Hittner, D. M. *Macromolecules* **2000**, *33*, 110.
(39) Dais, P. *Adv. Carbohydr. Chem. Biochem.* **1995**, *51*, 63−131.

MA001076I